Heliyon 10 (2024) e33487

Contents lists available at ScienceDirect

Heliyon

journal homepage: www.cell.com/heliyon

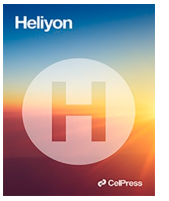

Research article

Spatiotemporal heterogeneity of the association between short-term exposure to carbon monoxide and COVID-19 incidence: A multistage time-series study in the continental United States

Jia Chen [a,b], Ping Lin [a], Ping Tang [a], Dajian Zhu [c], Rong Ma [d,*], Juan Meng [b,**]

[a] *Department of Otolaryngology - Head and Neck Surgery, The Second People's Hospital of Chengdu, Chengdu, 610000, China*
[b] *Department of Otorhinolaryngology - Head and Neck Surgery, West China Hospital, West China School of Medicine, Sichuan University, Chengdu, 610041, China*
[c] *Department of Otorhinolaryngology, The First People's Hospital of Shuangliu District / West China (Airport) Hospital Sichuan University, Chengdu, 610000, China*
[d] *People's Hospital of Xindu District, Chengdu, 610500, China*

A R T I C L E I N F O

Keywords:
COVID-19 incidence
Carbon monoxide
Post-pandemic era
Spatiotemporal pattern
Vaccination

A B S T R A C T

Background: Previous research has established carbon monoxide (CO) as a significant air pollutant contributing to coronavirus disease 2019 (COVID-19) transmission. The spatiotemporal heterogeneity in the relationship between short-duration CO exposure and COVID-19 incidence remain underexplored. Investigating such heterogeneity plays a crucial role in designing region-specific cost-effective public health policies, exploring the reasons for heterogeneity, and understanding the temporal trends in the association between CO and an emerging infectious disease such as COVID-19.

Methods: The 49 states of the continental United States (U.S.) were examined in this study. Initially, we developed time-series generalized additive models (GAMs) for each state to assess the preliminary correlation between daily COVID-19 cases and short-term CO exposure from April 1, 2020, to December 31, 2021. Subsequently, the correlations were compiled utilizing Leroux-prior-based conditional autoregression (LCAR) to achieve a smoothed spatial distribution. Finally, we integrated a time-varying component into the GAM and LCAR to analyze temporal correlations and illuminate the factors contributing to spatiotemporal heterogeneity.

Results: Our analysis revealed that, across the 49 states, a 10-ppb increase in CO concentration was associated with a 1.33 % (95%CI: 0.86%–1.81 %) increase in COVID-19 cases on average. Furthermore, spatial variability was noted, with weaker correlations observed in the central and southeastern regions, stronger associations in the northeastern regions, and negligible associations in the western regions. Temporally, the correlation was not significant from April 2020 to June 2021, but began to increase steadily thereafter until the end of 2021. Additionally, vaccination and temperature were determined to be potential causes contributing to the heterogeneity, indicating stronger positive associations in areas with higher vaccination rates and temperatures.

Conclusion: The findings of this study underscore the importance of monitoring CO pollution in the central and northeastern US, especially in the aftermath of the pandemic.

* Corresponding author. People's Hospital of Xindu District, Chengdu, 610500, China.
** Corresponding author. Department of Otorhinolaryngology - Head and Neck Surgery, West China Hospital, West China School of Medicine, Sichuan University, Chengdu, China.
E-mail addresses: 13881988335@163.com (R. Ma), mjmelinda@163.com (J. Meng).

https://doi.org/10.1016/j.heliyon.2024.e33487
Received 4 March 2024; Received in revised form 14 June 2024; Accepted 21 June 2024
Available online 25 June 2024

1. Background

Since December 2019, the severe acute respiratory syndrome coronavirus (SARS-CoV-2) has rapidly spread worldwide, marking an unprecedented global health crisis [1]. This virus, known for its exceptional capacity to evade the immune system, is highly contagious and has led to the devastating coronavirus disease 2019 (COVID-19) pandemic [2]. Despite being significantly underestimated, 769,806,130 COVID-19 cases had been documented as of August 16, 2023, resulting in 6,955,497 fatalities [3]. The COVID-19 pandemic has subsequently imposed a substantial burden on global health systems and populations [4].

Carbon monoxide (CO) is the most harmful byproduct of incomplete fossil fuel combustion [5]. In general, the level of carboxyhemoglobin (COHb) in the body is generally below 2 %; but due to CO's potent affinity with hemoglobin, the significantly rising level of COHb could lead to reduced oxygenation in both peripheral and cerebral tissues, manifesting symptoms such as chest discomfort, disorientation, headaches, weakness, coughing, shortness of breath, dyspnea, and in severe cases, loss of consciousness [6–8]. The diminished oxygenation also impairs the immune system, thus increasing the susceptibility to various diseases [9]. Although the underlying mechanisms have not been fully delineated, it is biologically plausible that short-term exposure to low levels of ambient CO is associated with increased daily mortality and cardiovascular or pulmonary disease morbidity [10,11]. Epidemiological studies have provided evidence regarding the association between ambient CO exposure and blood markers of inflammation and coagulation, including increased levels of C-reactive protein, intercellular adhesion molecule-1, and fibrinogen [12]; besides, Short-term CO exposure was also found to impair lung function in children and increase the blood pressure for women [13,14]. Therefore, CO is worthy of being regarded as an independent atmospheric pollutant for exploration.

According to a previous study evaluating the health impacts of air pollutants (CO, fine particulate matter, ozone, sulfur dioxide, and nitrogen dioxide), exposure to CO has been pinpointed as the most substantial marginal attributable burden among the five key air pollutants in the context of COVID-19 cases [15]. Currently, extensive epidemiological investigation has examined the correlation between short-term exposure to CO and the occurrence of COVID-19. Nevertheless, the findings of these investigations have been notably inconsistent. For instance, Kutralam-Muniasamy et al. [16] and Dragone et al. [17] showed that short-term CO exposure is highly correlated with the increase of COVID-19 incidence in Mexico City and Lombardy provinces, Italy, but Meo et al. [18] found negative and negligible correlations between short-term CO exposure and COVID-19 occurrence. Recently, a review ([19] revealed that a considerable proportion of the examined publications (61 %) found the relationship between CO exposure and COVID-19 incidence to be negligible or negative. Furthermore, the review highlighted that correlations varied significantly across different regions. The results underscore the importance of considering spatial variability in large-scale studies to avoid drawing inaccurate conclusions about the link between CO exposure and COVID-19 in some areas, which could have potentially profound implications for public health policy and interventions. Moreover, the review pointed out that the temporal variability in the association of CO exposure and COVID-19 over time could be attributed to human behavior modification, immunization campaigns, and viral mutations. Identifying these contributing factors to the temporal variation of associations is crucial for developing effective public health strategies that can be adapted to various phases of the pandemic response and might also provide insights into predicting future relationships. However, few studies have covered the spatiotemporal correlations between CO exposure for a short term and SARS-CoV2 infections.

By the end of December 2021, the United States (U.S.) reported 52 million COVID-19 cases and 840,000 fatalities, making it one of the countries most severely impacted by the pandemic. Variations in political and environmental factors lead to considerable differences among states in terms of epidemic prevention–control programs, as well as effect-modifying variables related to COVID-19 [20]. The relationship between CO exposure and COVID-19 incidence may demonstrate considerable spatiotemporal heterogeneity, influenced largely by these diverse factors. Despite a significant reduction in CO concentrations over the past few decades, with levels stabilizing at a relatively low average (~200 ppb) in recent years, certain local regions, such as California (CA), continue to face high CO concentrations due to frequent wildfires [21,22]. A previous study has uncovered that the health burden attributable to CO in relation to COVID-19 remains substantial in the U.S., surpassing the impacts of other air pollutants [15]. Thus, the spatiotemporal variability of CO-COVID-19 association within the U.S. should hold more attention when considering its implications for public health. Further, the availability of high-quality data from monitoring stations provides an opportunity for exploring the heterogeneity in the relationship between CO exposure and COVID-19 incidence within the U.S., where there are abundant medical supplies and a precise registration system.

In our research, we studied the spatial patterns of correlations between short-term CO exposure and cases of COVID-19 in the continental U.S. using daily confirmed COVID-19 cases along with CO concentration data. Additionally, we investigated the temporal fluctuation trajectory of the relationship between CO exposure and COVID-19 incidence and identified potential factors contributing to the spatiotemporal heterogeneity. Our findings suggest that understanding these patterns could facilitate the development of region-specific and time-specific public health policies for COVID-19 prevention, control, and air pollution management. Furthermore, the study further offers implications for the optimal locations and methods for performing cost-effective validation research utilizing individual-level data.

2. Methods

2.1. Data collection and processing

This study incorporated data from 49 states, including 48 native states and the District of Columbia, referred to here as a special

entity. We used two-letter abbreviations for each state to maintain clarity. A complete list of state names, their abbreviations, and geographical locations are provided in Table S1 as well as Figure S1.

Given the severly underestimated COVID-19 cases during the early and late phases of the pandemic, our analysis focused on the period from April 1, 2020 to December 31, 2021. Daily confirmed COVID-19 cases per state were compiled from the National Centers for Disease Control and Prevention (CDC). Corresponding state-level daily CO concentrations at 0.75° × 0.75° resolution were obtained from the fourth-generation ECMWF global reanalysis of atmospheric composition, available at https://ads.atmosphere.copernicus.eu/cdsapp#!/dataset/cams-global-reanalysis-eac4?tab=overview. State-level daily vaccination data, including percentage of the population that received at least one vaccine dose (PP1V) and percentage fully vaccinated (PPFV), were retrieved from the website https://covid.cdc.gov/covid-data-tracker/#datatracker-home. Meteorological data, including temperature, air pressure, and wind velocity, were collected from 64,346 monitoring stations, accessible at https://doi.org/10.7289/V5D21VHZ [23]. Population data at the state level for 2021 were acquired from the 24th census of the U.S., which can be accessed at https://www.census.gov/. The retrieved data for the study met the analytical criteria, with no instances of missing data throughout the specified study period.

A kriging interpolation approach with population weighting was utilized to achieve more accurate daily exposure data that considers the unevenly spatially distributed population. Initially, high-resolution meteorological data and CO concentrations were acquired using the standard kriging method based on a fine grid resolution of 1 km × 1 km [24]. The state-level statistics were then obtained by computing the average grid values for each state. Lastly, the daily average meteorological data per state were computed by averaging the population-weighted values of all states.

2.2. Statistical analysis

Because the traditional meta-analysis-based approaches do not account for the commonly-existed spatial dependencies among associations and lack the capability to assess temporal variations in these associations [25], we adopted a recently introduced conditional-autoregression-based strategy to assess the spatial pattern of the association between CO exposure COVID-19 incidence. Subsequently, we applied a modified time-varying strategy to investigate the temporal variation trend and explore the possible effect-modifying factors. The R Foundation for Statistical Computing version 4.2.1 was utilized to execute the analyses of statistical data. The statistical significance levels were set as $p < 0.05$ for the two-tailed test. The flow chart illustrating the analytical process is presented in Fig. 1.

2.2.1. Generalized additive model (GAM)

In the first stage, a standardized analytical procedure was utilized to obtain the preliminary estimation of the correlation between CO exposure for a short term and COVID-19 incidence for each state. Specifically, time-series GAMs were generated for each state with consistent model specifications:

$$Y_t \sim Quasi - Poisson(u_t),$$

$$ln(u_t) = \alpha + \beta CO_t + s_1(Temp_t) + s_2(AP_t) + \varphi Wind_t + s_3(Time_t) + Auto.term_t + DOW_t + Holiday_t, \quad (1)$$

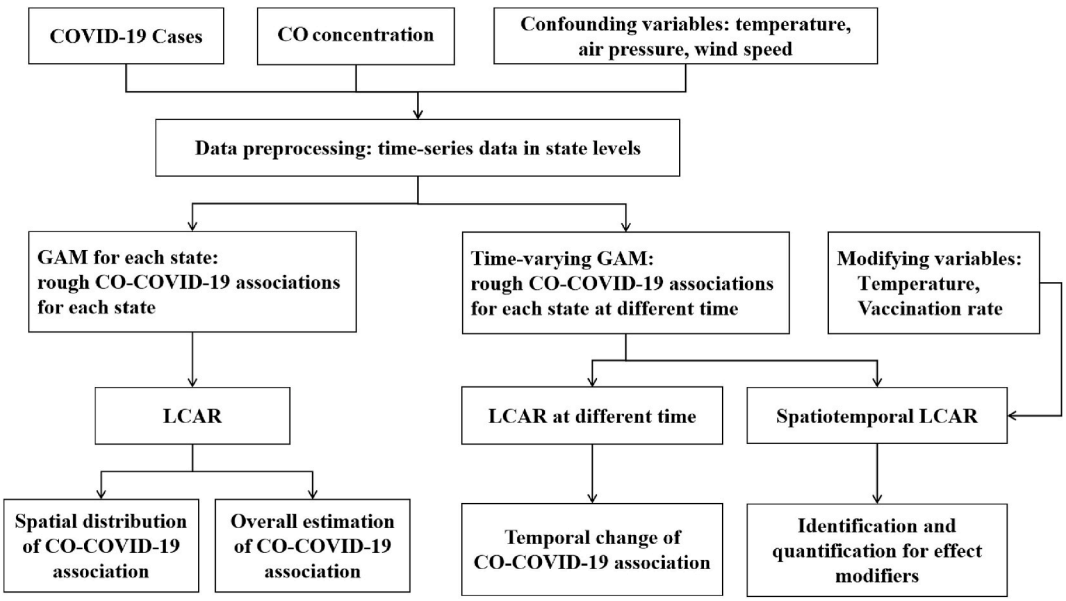

Fig. 1. The methodological flow chart of the spatiotemporal heterogeneity analysis for the CO-COVID-19 associations.

where Y_t denotes the daily case count at time t for a particular state with $E(Y_t) \equiv u_t$. Due to the over-dispersion observed in COVID-19 cases, a quasi-Poisson distribution was chosen as the fitting probability function. Here, α indicates the intercept and β reflects the strength of the association between CO exposure and COVID-19 incidence. CO_t represents the exponential moving average (EMA) of CO concentrations over a 0–14 days lag period [26,27], chosen based on the score of generalized cross-validation (Figure S2 in the Supplementary materials) and the time of incubation for SARS-COV-2. Additionally, $s_1(Temp_t)$ and $s_2(AP_t)$ capture the effects of temperature and air pressure, respectively, modeled using natural cubic splines with corresponding degrees of freedom (df) of 4 and 3. $Wind_t$ denotes the wind speed EMA with a 0–14 days lag. $s_3(Time_t)$ represents the natural cubic spline trend over the long period with a df value of 11/year. The Bayesian information criteria were utilized to optimize the selection of confounding variables and their respective df values. $Auto.term_t$ denotes the autoregressive term that reclaims the independence of errors due to the high contagiousness of COVID-19. The impacts of weekends and holidays are shown by DOW_t and $Holiday_t$. The Supplementary materials (Table S2 and Figure S3) present the details about the selection of parameters.

2.2.2. Leroux-prior-based conditional autoregression (LCAR)

The second phase involved the use of an LCAR model to achieve spatial smoothness for the parameters, which were derived from the estimates of state-specific correlations in equation (1), i.e., the coefficients $\widehat{\beta}_i$ and the standard error $\widehat{\sigma}_i$. Compared with the traditional meta-analysis method, LCAR can sufficiently utilize the spatial dependencies, thus yielding results with higher stability and accuracy. The LCAR model is established below:

$$\widehat{\beta}_i \sim \mathrm{N}\left(\beta_i', \widehat{\sigma}_i^2\right),$$

$$\beta_i' = \eta + \xi_i,$$

$$\boldsymbol{\xi} \sim \mathrm{MN}\left(\mathbf{0}, [\tau \mathbf{W}]^{-1}\right), \tag{2}$$

$$\mathbf{W} = \rho \mathbf{R} + (1 - \rho)\mathbf{I}, \tag{3}$$

where β_i' denotes the true associations for state i. The symbol η denotes the average associations for all states and ξ_i (the ith element of $\boldsymbol{\xi}$) represents the spatial heterogeneity. As such, $\boldsymbol{\xi}$ follows a multivariate normal distribution as shown in formula (2) where τ illustrates the precision parameter. The spatial dependency based on Leroux prior is shown by $\mathbf{W}$, with the intensity of this dependence measured by ρ. The symmetric matrix denoted by $\mathbf{R}$ is a derivative of the spatial adjacent association. $\mathbf{I}$ is an identity matrix. The estimated value of β_i', labeled as $\widehat{\beta}_i'$, was estimated utilizing the Integrated Nested Laplace Approximations [28,29]. The spatial distribution of CO–COVID-19 correlation was obtained based on $\widehat{\beta}_i'$.

2.2.3. Time-varying GAM-LCAR

Given the dynamic nature of the immune evasive capability of SARS-CoV-2, vaccination rates, and preventive measures, we developed a modified time-varying GAM-LCAR to assess the temporal fluctuation patterns in the correlation between CO exposure and COVID-19 incidence and identify potential effect-modifying factors.

Initially, we developed a time-varying GAM to incorporate nonlinear interactions between CO exposure and time, with the model (1) serving as the point of reference. For each state, the time-varying GAM was generated as

$$ln(u_t) = \alpha + s_1(Temp_t) + s_2(AP_t) + \varphi Wind_t + s_3(Time_t) + Auto.term_t + DOW_t + Holiday_t + s_4(Time_t) * CO_t. \tag{4}$$

In equation (4), $s_4(Time_t)$ reflects the natural cubic spline of time, for which the df is 3, illustrating the linear impact of CO on the incidence of COVID-19 at time t, i.e., $s_4(Time_t) = \beta_t$. Consequently, the natural cubic spline for $s_4(Time_t)$ assures a continual change while allowing for a nonlinear evolution of the relationship change over time, which is more reasonable because the associations between two adjacent time points tend to be similar. Subsequently, we pooled the association parameter from the time-varying GAMs across states for each specific time point t using an LCAR model, as detailed in Section 2.2.2, to compute time-specific average associations.

The following spatiotemporal LCAR model was developed to determine if temperature and vaccination rates modify the association:

$$\widehat{\beta}_{it} \sim N\left(\beta_{it}', \widehat{\sigma}_{it}^2\right),$$

$$\beta_{it}' = \eta + \theta x_{it} + \xi_i + \gamma_t, \tag{5}$$

$$\boldsymbol{\xi} \sim \mathrm{MN}\left(\mathbf{0}, [\tau \mathbf{W}]^{-1}\right),$$

$$\gamma_t \,\Big|\, \gamma_{t-1} \sim N\left(\gamma_{t-1}, \sigma_\gamma^2\right), \tag{6}$$

where $\widehat{\beta}_{it}$ indicates the estimate of the association parameter from the time-varying GAM at time t for state i, and the corresponding standard error is denoted by $\widehat{\sigma}_{it}$. x_{it} represents the vaccine or temperature while θ indicates the magnitude of the modification impact in linear terms. The spatiotemporal autocorrelations are denoted by ξ_i and γ_t, which were distinguished, respectively, by the implementation of an LCAR-based prior as shown in equation (3) and a random walk prior as shown in formula (6). In addition, we examined the nonlinear impact of modification by adjusting equation (5) as follows: $\beta'_{it} = \eta + s(x_{it}) + \xi_i + \gamma_t$, where $s(x_{it})$ represents a natural cubic spline function, for which the df is 3.

3. Results

3.1. Descriptive results

Fig. 2 delineates the temporal pattern of the vaccination rate and the spatial patterns of CO exposure, COVID-19 incidence, and vaccination rates in the U.S. Notably, an aggregate of 52,250,191 cases of confirmed COVID-19 cases were confirmed throughout the 49 continental states of the U.S. between April 1, 2020 and December 31, 2021. Fig. 2A illustrates the geographical distribution of these cases, highlighting CA, Texas (TX), and Florida (FL) as the states with the highest cumulative case numbers. An average of 16.63 % of the population in these states had been reported as COVID-19 cases by December 31, 2021. Furthermore, the COVID-19 incidence across states varied between 8 % and 23 %, as illustrated in Fig. 2B. The central and eastern regions of the country exhibited higher incidence rates, whereas Oregon, Washington, and some northern states recorded lower incidence rates. Fig. 2C presents the spatial variation in CO concentrations, with state-specific average concentrations ranging from 151.53 to 348.03 ppb. A comparative analysis of CO concentration in the U.S. with those in other countries (Figure S11) uncovered the western region in the U.S. exhibited higher CO

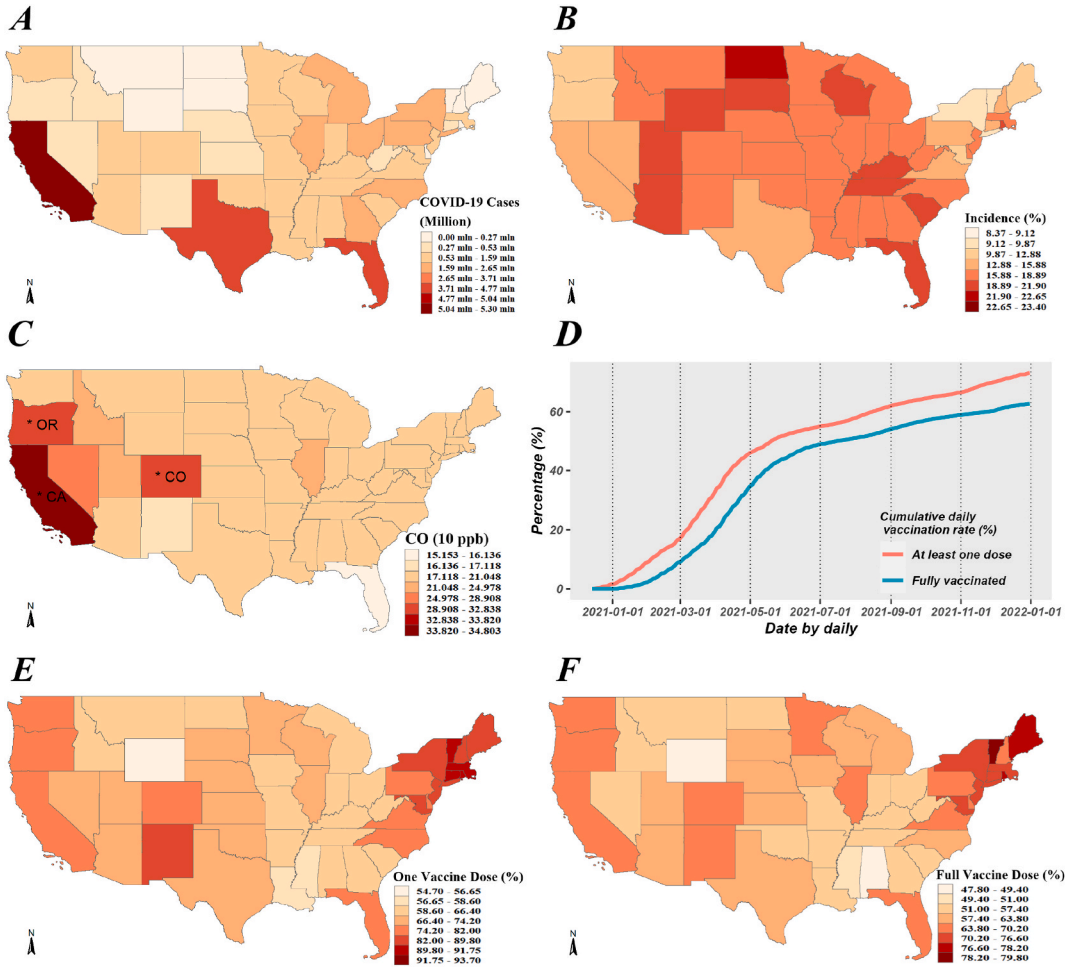

Fig. 2. Spatial description of COVID-19 incidence, carbon monoxide exposure, and vaccination rates. Fig. 2A and B exhibits the cumulative COVID-19 cases and incidence from April 1, 2020 to December 31, 2021, respectively. Fig. 2C exhibits the average daily CO concentrations between observation period, in which asterisks mark (*) the three states with the highest average concentrations of CO. Fig. 2D exhibits the time trends of vaccination rates. Fig. 2E and F exhibit the cumulative vaccination rates for one or full dose in each state, respectively.

concentrations than most other states, which may be ascribed to the frequent mountain fires in CA. Conversely, CO concentrations in other regions of the U.S. were relatively lower.

The mean coverage rate for PP1V was recorded at 72.23 %, while that for PPFV reached 61.70 % by December 31, 2021. Fig. 2D illustrates the temporal trend of increasing vaccine coverage rates. Fig. 2E and F further detail the spatial distribution of PP1V and PPFV, respectively. This variability underscores the potential importance of examining how vaccination rates may influence the association between CO exposure and COVID-19 incidence.

3.2. Spatial distribution of the CO–COVID-19 association

As depicted in Fig. 3, short-term CO exposure was positively linked to a greater risk of COVID-19 incidence in most northeastern states of the U.S. Specifically, a 10-ppb increase in CO levels was associated with a 1.33 % increase in COVID-19 cases (95%CI: 0.86%–1.81 %). Predictably, the strength of this correlation varied significantly across the 49 states, with relative risks (RRs) corresponding to a 10-ppb rise in CO ranging from 0.98 to 1.04. Notably, significant positive correlations were observed in a majority of northeastern states, including Minnesota, Iowa, Wisconsin, Massachusetts, Vermont, Connecticut, New York (NY), New Jersey, Pennsylvania, Ohio, Maine, and Rhode Island. Conversely, significant negative correlations were recorded in southeastern and southwestern states, particularly in CA and FL.

The lack of significant correlations in many states located in the western, central, and southeastern regions could be attributed to insufficient statistical power corresponding to the individual state level. Therefore, a meta-analysis was implemented to combine the impacts in 15 southern, 11 western, and 9 central states, where correlations were found to be insignificant. The homogeneity of correlations within these regions was supported by the I^2 statistics, as depicted in Fig. 4. Hence, the fixed-effect models were used to synthesize the effects. According to the obtained data, the average impacts are weak but significant in the central and southeastern parts, with RRs of 1.012 (95%CI: 1.006–1.019) and 1.005 % (95%CI: 1.000%–1.009 %), respectively. Nevertheless, the average impact remained insignificant in the western region, with an RR of 1.001 (95 % CI: 0.996–1.006).

The validity of incorporating spatial dependency through the LCAR-based method was evaluated utilizing the traditional meta-analysis-based two-stage and stratified techniques. Unlike meta-analysis, which assumes uniform correlation strength across all states, and stratified techniques, which deny any inter-state similarities, the LCAR approach acknowledges geographical variations. The performance of each model was evaluated using the deviance information criterion (DIC) [30] and the logarithmic score (LS) [31], with lower values indicating superior model performance. The LCAR-based approach illustrated the highest performance levels, as evidenced by the lowest DIC values (-245.59, -238.03, and -216.59) and LS values (-120.47, -111.10, and -70.68) compared to the meta-analysis and stratified approaches, respectively.

3.3. Temporal variations in associations and the modifying impacts of vaccination and temperature

As depicted in Fig. 5, we corroborated the time-specific average associations between CO exposure and COVID-19 incidence across all states utilizing the time-varying GAM-LCAR method. A period of stability was noted from April 2020 to June 2021, during which the RR remained close to 1, indicating no significant association. Thereafter, the association exhibited a marked increase from June 2021 to December 2021, culminating in a maximum RR of 1.050 (95%CI: 1.036–1.064).

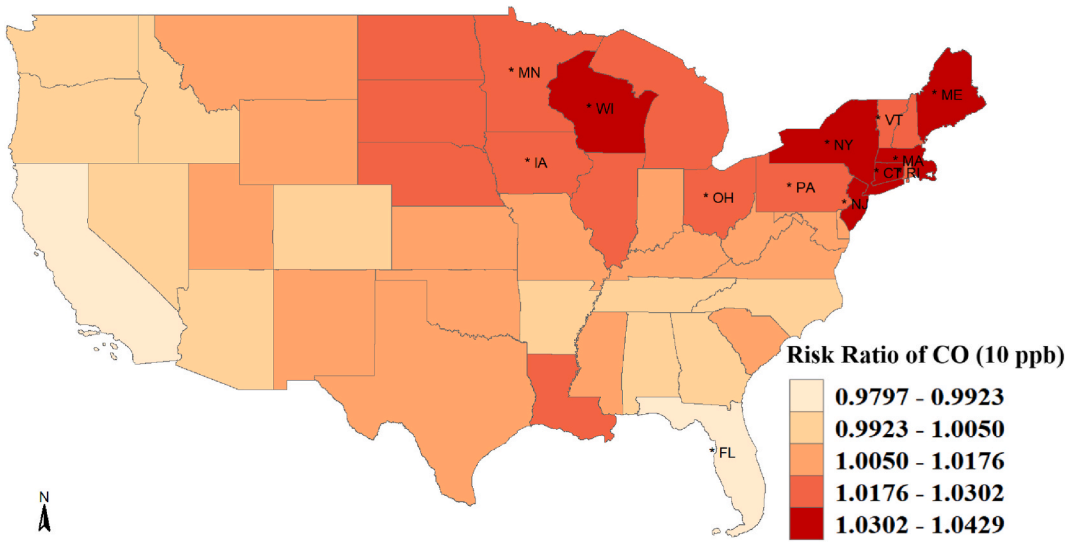

Fig. 3. Spatial distribution of association between short-term exposure to CO and the incidence of COVID-19. The asterisk mark (*) denotes a statistically significant relative risk (RR) ($P < 0.05$).

A

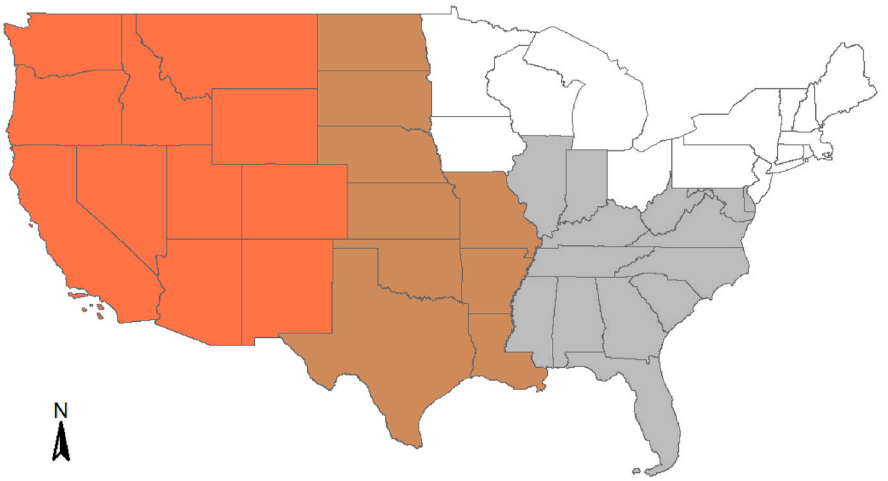

B

Study	TE	SE(TE)		95%-CI	Weight (common)	Weight (random)
Idaho	0.9997	0.01	1.000	[0.986; 1.013]	13.3%	13.3%
New Mexico	1.0092	0.01	1.009	[0.986; 1.032]	4.7%	4.7%
California	0.9908	0.01	0.991	[0.971; 1.011]	6.3%	6.3%
Oregon	0.9994	0.01	0.999	[0.984; 1.015]	9.7%	9.7%
Washington	1.0003	0.01	1.000	[0.985; 1.016]	10.0%	10.0%
Utah	1.0051	0.01	1.005	[0.988; 1.022]	8.4%	8.4%
Colorado	1.0031	0.01	1.003	[0.983; 1.023]	6.1%	6.1%
Wyoming	1.0083	0.01	1.008	[0.988; 1.029]	5.8%	5.8%
Nevada	0.9985	0.01	0.999	[0.982; 1.015]	8.8%	8.8%
Montana	1.0163	0.01	1.016	[0.996; 1.036]	6.1%	6.1%
Arizona	0.9974	0.01	0.997	[0.987; 1.008]	20.9%	20.9%
Fixed effect model			**1.001**	**[0.996; 1.006]**	**100.0%**	--
Random effects model			**1.001**	**[0.996; 1.006]**	--	**100.0%**

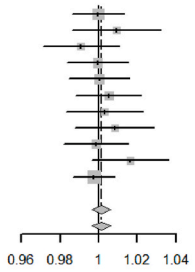

Heterogeneity: $I^2 = 0\%$, $\tau^2 = 0$, $p = 0.88$

C

Study	TE	SE(TE)		95%-CI	Weight (common)	Weight (random)
Nebraska	1.0176	0.01	1.018	[0.997; 1.039]	10.9%	10.9%
Louisiana	1.0213	0.01	1.021	[0.999; 1.044]	9.2%	9.2%
Texas	1.0174	0.01	1.017	[0.995; 1.040]	9.4%	9.4%
Oklahoma	1.0120	0.01	1.012	[0.994; 1.030]	15.0%	15.0%
North Dakota	1.0200	0.01	1.020	[0.995; 1.045]	7.8%	7.8%
Arkansas	1.0022	0.01	1.002	[0.985; 1.019]	16.3%	16.3%
Missouri	1.0059	0.01	1.006	[0.987; 1.024]	13.9%	13.9%
Kansas	1.0084	0.01	1.008	[0.983; 1.033]	7.6%	7.6%
South Dakota	1.0183	0.01	1.018	[0.996; 1.040]	9.9%	9.9%
Fixed effect model			**1.012**	**[1.006; 1.019]**	**100.0%**	--
Random effects model			**1.012**	**[1.006; 1.019]**	--	**100.0%**

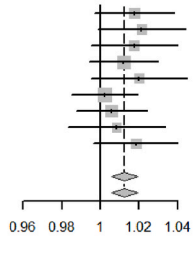

Heterogeneity: $I^2 = 0\%$, $\tau^2 = 0$, $p = 0.89$

D

Study	TE	SE(TE)		95%-CI	Weight (common)	Weight (random)
West Virginia	1.0132	0.01	1.013	[0.995; 1.031]	5.8%	6.0%
Florida	0.9797	0.01	0.980	[0.961; 0.998]	5.7%	5.9%
Illinois	1.0183	0.01	1.018	[0.999; 1.037]	5.3%	5.6%
Maryland	1.0163	0.01	1.016	[0.998; 1.034]	6.0%	6.2%
North Carolina	1.0008	0.01	1.001	[0.987; 1.015]	9.8%	9.3%
Delaware	1.0160	0.01	1.016	[0.994; 1.038]	3.9%	4.2%
Georgia	0.9972	0.01	0.997	[0.984; 1.011]	10.6%	9.9%
Alabama	0.9960	0.01	0.996	[0.980; 1.012]	7.2%	7.2%
South Carolina	1.0056	0.01	1.006	[0.993; 1.019]	11.5%	10.5%
Tennessee	0.9995	0.01	0.999	[0.984; 1.015]	7.8%	7.8%
Kentucky	1.0058	0.01	1.006	[0.990; 1.022]	7.5%	7.5%
Mississippi	1.0073	0.01	1.007	[0.992; 1.022]	8.4%	8.2%
Indiana	1.0168	0.01	1.017	[0.993; 1.041]	3.3%	3.7%
Virginia	1.0100	0.01	1.010	[0.991; 1.029]	5.2%	5.5%
District of Columbia	1.0199	0.02	1.020	[0.989; 1.051]	2.0%	2.3%
Fixed effect model			**1.005**	**[1.000; 1.009]**	**100.0%**	--
Random effects model			**1.005**	**[1.000; 1.010]**	--	**100.0%**

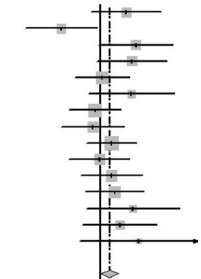

Heterogeneity: $I^2 = 22\%$, $\tau^2 < 0.0001$, $p = 0.21$

(caption on next page)

Fig. 4. Meta-analyses for the associations between CO and COVID-19 incidence in insignificant regions. Fig. 4A exhibits the spatial distribution of states in the three meta-analyses, Fig. 4B, C and D exhibit the meta-analysis results in the western (orange), middle-northern (brown) and southeastern (grey) states respectively. Note that the standard of subregion division was based on the combination of the spatial locations of states and whether the RR values were statistically significant.

The spatiotemporal LCAR model, depicted in Table 1, investigated the linear modifying influence of temperature and vaccination on the CO–COVID-19 correlation. An increase in the vaccination rate by 1 % was associated with a 0.23 % and 0.29 % rise in the RR of CO exposure for PP1V and PPFV, respectively, indicating a significant modification of the association. The modifying impact of temperature on the correlation was weak, although it reached significance, with a 1 °C rise in temperature resulting in a 0.05 % increment in the RR. In addition, the nonlinear modifying impacts of vaccinations and temperature on the CO–COVID-19 association were examined (Fig. 6). At higher vaccination rates, both PP1V and PPFV considerably enhanced the negative influence of CO exposure on COVID-19 incidence. Conversely, at low vaccination rates (<53 % for PP1V and <70 % for PPFV), the modifying effects were not significant. The modifying impact of temperature on the CO-COVID-19 association was predominantly linear.

3.4. Sensitivity analysis

In the sensitivity analysis, we examined the potential nonlinear relationship between daily COVID-19 cases and short-term CO exposure. Accordingly, we adopted a natural cubic spline model with a df of 3 to characterize any nonlinear dynamics in the CO–COVID-19 relationship. As evidenced in Fig. 7, the CO–COVID-19 correlation was approximately linear, indicating that the linear hypothesis was justified in the primary analysis. Moreover, we conducted additional sensitivity analyses to account for adjusting for the seasonal trends and relative humidity. The results, as depicted inFigure S5–S10 of the Supplementary materials, demonstrated that the association remained consistent and stable, even after accounting for these factors.

4. Discussion

This study is the first to examine the spatiotemporal variability in the correlation between short-term exposure to CO and the risk of COVID-19. We uncovered notable spatial heterogeneity in this relationship; specifically, the correlation between CO exposure and COVID-19 incidence was weak and insignificant in the central, western, and southeastern states. In contrast, significant positive relationships were predominantly found in the central and northeastern regions. The strength of CO–COVID-19 correlation substantially rose over time in the post-pandemic era. Vaccination rates and temperature were pinpointed as major predisposing factors contributing to the spatiotemporal heterogeneity, highlighting regions and periods of heightened sensitivity where CO exposure may worsen COVID-19 transmission. Such insights are crucial for understanding the temporal trajectory of the link between CO exposure and susceptibility to infectious diseases, including COVID-19.

The data from 49 states revealed that a 10-ppb increment in CO concentrations corresponded to a 1.33 % rise (95%CI: 0.86%–1.81 %) in COVID-19 cases on average. Our finding further provides evidence that short-term CO exposure increases the incidence of COVID-19, which concurs with existing literature [19]. Spatial analysis revealed a notably robust CO–COVID-19 correlation in the northeastern states such as Wisconsin, New Jersey, NY, Connecticut, Massachusetts, and Maine. The robustness of this correlation is unlikely to be caused by the type-I error introduced by multiple testing or random spatial permutations, suggesting that an epidemiological mechanism may underlie these findings. Furthermore, our findings suggest that the intensity of the CO-COVID-19 relationship does not solely depend on average CO concentrations. States with higher CO concentrations did not necessarily exhibit the strongest exposure-response relationships, indicating that other factors, such as local meteorological conditions, demographic characteristics, and behavioral practices, may play significant roles. Understanding these interactions is essential for developing targeted public health interventions and policies that can effectively mitigate the impacts of air pollution on infectious disease transmission.

Conversely, most states situated in the western, central, and southern areas had weak CO–COVID-19 correlations that were insignificant, with some even exhibiting negative correlations. This observation does not undermine the overall conclusion that CO exposure facilitates the risk of COVID-19 transmission. Notably, the lack of significant findings in these regions could be attributed to

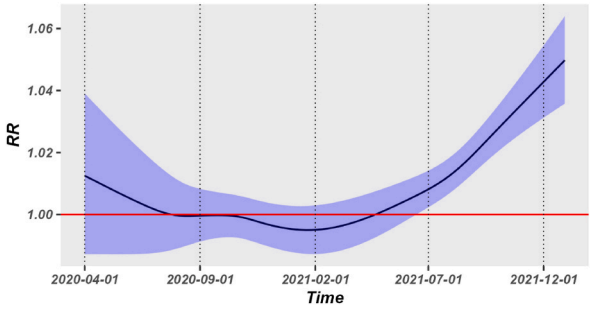

Fig. 5. Temporal patterns of the association between short-term CO exposure and COVID-19 incidence over time.

Table 1
Linear modification effect of vaccination and temperature on the association between short-term CO exposure and COVID-19 incidence.

Variables	Relative risk				
	Mean[a]	SD	Median	95%CI lower	95%CI higher
PP1V	1.00225	0.00012	1.00225	1.00202	1.00248
PPFV	1.00294	0.00012	1.00294	1.00272	1.00317
Temperature	1.00052	0.00010	1.00052	1.00034	1.00071

Note.

[a] This value is $e^{\hat{\theta}}$ where $\hat{\theta}$ is the estimated parameter in model (5).

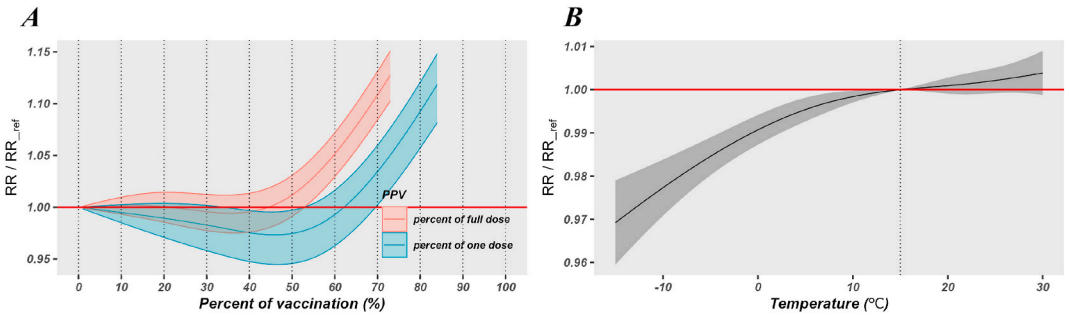

Fig. 6. Temperature and vaccination's nonlinear modifying impact on the CO-COVID-19 association. Fig. 6A exhibits the modification effect of vaccination rates, red line indicates the percentage of full dose vaccination rate (PPFV) and blue line indicates the percentage of one dose vaccination rate (PP1V); and Fig. 6B exhibits the modification effect of daily temperature.

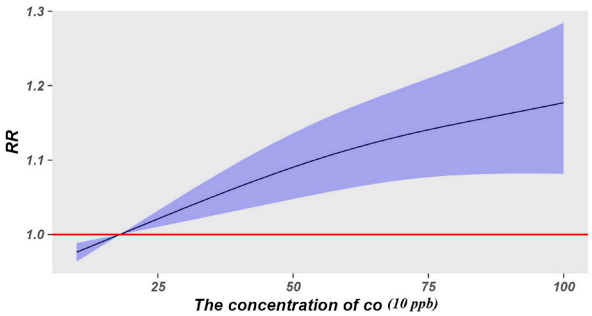

Fig. 7. The average nonlinear associations between short-term CO exposure and COVID-19 incidence.

insufficient statistical power when analyzing data on a state-by-state basis. Alternatively, we implemented an additional meta-analysis for the western, central, and southeastern regions based on their RR values and spatial location. The obtained data unveiled that the average impacts of CO exposure on COVID-19 incidence remained significant in the central and southeastern states, implying that the adverse impacts of CO in the two regions should not be disregarded. However, in the western region, the average impact remains insignificant. Interestingly, several counties exhibited a negative correlation, some of which was significant. We hypothesize that the lack of significant impact in the western states may not be attributable to low statistical power. Given the possibility of unobserved confounding variables and the risk of ecological fallacy, more individual-based investigation is required to verify our findings. Due to the significant spatial heterogeneity in the association, we also used the recently proposed estimation-error-based spatial scan statistic to detect the association-clustered region [32,33]. Results showed that no clustering region was detected, which may owe to the insufficient power when the number of states was relatively small.

Our analysis revealed a noteworthy temporal fluctuation pattern in the CO–COVID-19 correlation throughout the pandemic. This pattern can be categorized into two stages: stage 1, largely defined by a consistently weak and insignificant association; and stage 2, wherein the association grew significantly over time. This period was characterized by widespread public concern over the pandemic, which significantly affected daily communications and led to increased protective measures such as reducing outside activities. These behaviors likely reduced individuals' actual exposure to CO, resulting in a minimal correlation between outdoor CO levels and COVID-19 infection rates. In contrast, the second phase saw a marked strengthening of the CO–COVID-19 correlation. This change coincided with the rollout and widespread acceptance of COVID-19 vaccinations, which paradoxically led to a relaxation in adherence to

preventive measures, such as outdoor activities and social distancing. Hence, people's exposure to environmental pollutants, including CO, increased, intensifying the CO–COVID-19 correlation [34]. The post-epidemic period witnessed a stronger link between CO exposure and COVID-19, which may be attributed to the heightened susceptibility to the consequences of the pandemic, such as compromised immunity, more frequent outdoor exposure, and the increase of pollutant concentration caused by the recovery of normal production and life. The present temporal study underscores the influence of behavioral changes and public health awareness on the relationship between environmental contaminants and COVID-19 incidence. These insights have profound implications for public health strategies.

In the context of a new pandemic, people's behaviors often follow a consistent pattern: initially reducing social activities and avoiding crowds, then gradually resuming normal interactions as vaccination rates increase and acquired immunity increases. This observed temporal trend in the CO–COVID-19 association may also be referenced for managing future pandemics. During an extensive emerging infectious disease epidemic cycle, such as that of COVID-19, it is crucial for governments to strengthen public awareness about protective measures and control air pollution to mitigate the impact of environmental contaminants on the disease, especially in the post-epidemic phase compared to the epidemic and pre-epidemic phases.

Based on the flexible LCAR, the analytical technique in our work enabled adequate characterization of the possible spatial autocorrelation and utilized a modified time-varying GAM-LCAR to elucidate the temporal patterns of the CO–COVID-19 correlation. This approach also facilitated the examination of various factors contributing to observed spatiotemporal variability. The utility of this analysis strategy extends beyond our current focus, offering a versatile tool for other similar studies investigating the short-term correlation between environmental factors and public health outcomes. The substantial spatiotemporal heterogeneity in the correlation between CO exposure and COVID-19 incidence observed in the U.S. suggested that similar patterns of variability might be observed in other countries, particularly those covering extensive geographical areas. Thus, exploring the spatial heterogeneity of the CO–COVID-19 correlation across different countries could yield valuable insights.

However, several limitations must be acknowledged. Firstly, the reliance on interpolated CO concentrations from fixed environmental monitoring centers, rather than direct individual monitoring, might have introduced measurement inaccuracies about the actual exposure levels [35]. Secondly, the underreporting of COVID-19 cases during the early stages of the pandemic may have skewed the analysis due to difficulties in detecting viral nucleic acids [36]. Thirdly, the potential impact of SARS-CoV-2 variants that evolved during COVID-19 on the link between CO exposure and COVID-19 was not accounted for in our analysis. Hence, additional research that focuses on individual-level or quasi-experimental data is warranted to validate our findings.

Despite these limitations, our study highlights strategic approaches to conducting individual-based research. For instance, future investigations could focus on areas of high sensitivity, such as NY, Massachusetts, New Jersey, and Maine, to examine the adverse impacts of CO exposure on COVID-19 risk more precisely. Additionally, studies conducted during later vaccination phases could provide insights into the drivers of temporal heterogeneity. Comparative studies in regions with varying levels of vulnerability, such as NY and FL, could present a promising strategy for examining the possible factors underlying spatial differences in the CO–COVID-19 correlation.

5. Conclusion

This study is the first investigation of the spatiotemporal relationship between short-term CO exposure and COVID-19 incidence in the continental U.S. The evaluation of the data from 49 states revealed that a 10-ppb increase in CO levels is associated with a 1.33 % increase in COVID-19 cases. The findings highlight considerable spatial heterogeneity in the CO–COVID-19 correlations: strong in the northeastern regions, weak in the central and southeastern parts, and insignificant in the western parts. Temporally, the CO–COVID-19 correlation presented no significance from April 2020 to June 2021, but a gradual increase was noted from June 2021 to the end of 2021. Furthermore, our findings highlight the pivotal roles of vaccination rates and temperature in facilitating the spatiotemporal heterogeneity in the CO–COVID-19 association, which tends to become stronger at high temperature and vaccination rate. The research implications are particularly relevant for the northeastern U.S. during the post-pandemic period, where CO pollution warrants increased attention.

Ethics approval and consent to participate

This study did not involve any individual participant data. The Ethics Committee of Sichuan University affirmed that ethical approval was required for this study.

Consent for publication

Not applicable.

Data availability

The COVID-19 data can be publicly available from the Centers for Disease Control and Prevention, via https://covid.cdc.gov/covid-data-tracker/#datatracker-home. The daily Carbon Monoxide concentrations were from the fourth-generation ECMWF global reanalysis of atmospheric composition, which is publicly available at https://ads.atmosphere.copernicus.eu/cdsapp#!/dataset/cams-global-reanalysis-eac4?tab=overview.

Funding

This work was supported by Chengdu, Sichuan Province Health Commission Project (grant number: 2023301).

CRediT authorship contribution statement

Jia Chen: Writing – original draft, Formal analysis, Conceptualization. **Ping Lin:** Writing – review & editing, Visualization, Data curation. **Ping Tang:** Writing – review & editing, Data curation. **Dajian Zhu:** Writing – review & editing, Visualization, Data curation. **Rong Ma:** Writing – review & editing, Writing – original draft, Formal analysis. **Juan Meng:** Writing – review & editing, Methodology, Conceptualization.

Declaration of competing interest

The authors declare that they have no known competing financial interests or personal relationships that could have appeared to influence the work reported in this paper.

Acknowledgment

Special thanks are extended to the National Centers for Disease Control and Prevention for collecting and making publicly available the state-specific daily confirmed COVID-19 case datasets in the United States. We also thank Bullet Edits Limited for the linguistic editing and proofreading of the manuscript.

Appendix A. Supplementary data

Supplementary data to this article can be found online at https://doi.org/10.1016/j.heliyon.2024.e33487.

References

[1] M. Antonelli, et al., Risk of long COVID associated with delta versus omicron variants of SARS-CoV-2, Lancet 399 (10343) (2022) 2263–2264.
[2] G. Mooney, The dangers of ignoring history lessons during a pandemic, Ann. Intern. Med. 174 (4) (2021) 556–557.
[3] WHO, Coronavirus (Covid-19) Dashboard (2023). *https://covid19.Who.Int*. (Accessed 16 August 2023).
[4] M. Bushman, et al., Population impact of SARS-CoV-2 variants with enhanced transmissibility and/or partial immune escape, Cell 184 (26) (2021) 6229–6242.e18.
[5] Z. Yuan, et al., Carbon monoxide signaling: examining its engagement with various molecular targets in the context of binding affinity, concentration, and biologic response, Pharmacol. Rev. 74 (3) (2022) 823–873.
[6] P. Barn, et al., A review of the experimental evidence on the toxicokinetics of carbon monoxide: the potential role of pathophysiology among susceptible groups, Environ. Health 17 (1) (2018) 13.
[7] C. Reboul, et al., Carbon monoxide pollution aggravates ischemic heart failure through oxidative stress pathway, Sci. Rep. 7 (2017) 39715.
[8] S. Zevin, et al., Cardiovascular effects of carbon monoxide and cigarette smoking, J. Am. Coll. Cardiol. 38 (6) (2001) 1633–1638.
[9] I. Manisalidis, et al., Environmental and health impacts of air pollution: a review, Front. Public Health 8 (2020) 14.
[10] K. Chen, et al., Ambient carbon monoxide and daily mortality: a global time-series study in 337 cities, Lancet Planet. Health 5 (4) (2021) e191–e199.
[11] M.A. Bind, et al., Air pollution and markers of coagulation, inflammation, and endothelial function: associations and epigene-environment interactions in an elderly cohort, Epidemiology 23 (2) (2012) 332–340.
[12] R. Rückerl, et al., Associations between ambient air pollution and blood markers of inflammation and coagulation/fibrinolysis in susceptible populations, Environ. Int. 70 (2014) 32–49.
[13] T. Männistö, et al., Acute air pollution exposure and blood pressure at delivery among women with and without hypertension, Am. J. Hypertens. 28 (1) (2015) 58–72.
[14] D. Ierodiakonou, et al., Ambient air pollution, lung function, and airway responsiveness in asthmatic children, J. Allergy Clin. Immunol. 137 (2) (2016) 390–399.
[15] B. Feng, et al., Mapping the long-term associations between air pollutants and COVID-19 risks and the attributable burdens in the continental United States, Environ. Pollut. 324 (2023) 121418.
[16] G. Kutralam-Muniasamy, et al., Impacts of the COVID-19 lockdown on air quality and its association with human mortality trends in megapolis Mexico City, Air Qual Atmos Health 14 (4) (2021) 553–562.
[17] R. Dragone, et al., Analysis of the chemical and physical environmental aspects that promoted the spread of SARS-CoV-2 in the lombard area, Int. J. Environ. Res. Publ. Health 18 (3) (2021).
[18] S.A. Meo, et al., Effect of environmental pollutants PM-2.5, carbon monoxide, and ozone on the incidence and mortality of SARS-COV-2 infection in ten wildfire affected counties in California, Sci. Total Environ. 757 (2021) 143948.
[19] A. Bhaskar, et al., A literature review of the effects of air pollution on COVID-19 health outcomes worldwide: statistical challenges and data visualization, Annu. Rev. Publ. Health 44 (2023) 1–20.
[20] L. Becchetti, et al., Understanding the heterogeneity of COVID-19 deaths and contagions: the role of air pollution and lockdown decisions, J. Environ. Manag. 305 (2022) 114316.
[21] S. Yu, L. Hsueh, Do wildfires exacerbate COVID-19 infections and deaths in vulnerable communities? Evidence from California, J. Environ. Manag. 328 (2023) 116918.
[22] H. Chen, et al., Cardiovascular health impacts of wildfire smoke exposure, Part. Fibre Toxicol. 18 (1) (2021) 2.
[23] M.J. Menne, et al., An overview of the global historical climatology network-daily database, J. Atmos. Ocean. Technol. 29 (7) (2012) 897–910.
[24] F. Susanto, P. de Souza, J. He, Spatiotemporal interpolation for environmental modelling, Sensors 16 (8) (2016).
[25] C. Liu, et al., Ambient particulate air pollution and daily mortality in 652 cities, N. Engl. J. Med. 381 (8) (2019) 705–715.

[26] J.A. Backer, D. Klinkenberg, J. Wallinga, Incubation period of 2019 novel coronavirus (2019-nCoV) infections among travellers from Wuhan, China, 20-28 January 2020, Euro Surveill. 25 (5) (2020).
[27] N. Zaki, E.A. Mohamed, The estimations of the COVID-19 incubation period: a scoping reviews of the literature, J Infect Public Health 14 (5) (2021) 638–646.
[28] H. Rue, S. Martino, N. Chopin, Approximate Bayesian inference for latent Gaussian models by using integrated nested Laplace approximations, J. Roy. Stat. Soc. B 71 (2) (2009) 319–392.
[29] F. Lindgren, H. Rue, Bayesian spatial modelling with R-INLA, J. Stat. Software 63 (2015) 1–25.
[30] D.J. Spiegelhalter, et al., Bayesian measures of model complexity and fit, J. Roy. Stat. Soc. B 64 (4) (2002) 583–639.
[31] T. Gneiting, A.E. Raftery, Strictly proper scoring rules, prediction, and estimation, J. Am. Stat. Assoc. 102 (477) (2007) 359–378.
[32] W. Wang, et al., Detecting the spatial clustering of exposure-response relationships with estimation error: a novel spatial scan statistic, Biometrics 79 (4) (2023) 3522–3532.
[33] W. Wang, et al., Using a novel strategy to investigate the spatially autocorrelated and clustered associations between short-term exposure to PM(2.5) and mortality and the attributable burden: a case study in the Sichuan Basin, China, Ecotoxicol. Environ. Saf. 264 (2023) 115405.
[34] P. Ngamchaliew, et al., Changes in preventive behaviour after COVID-19 vaccination in Thailand: a cross-sectional study, BMC Publ. Health 22 (1) (2022) 2039.
[35] P.J. Villeneuve, M.S. Goldberg, Methodological considerations for epidemiological studies of air pollution and the SARS and COVID-19 coronavirus outbreaks, Environ. Health Perspect. 128 (9) (2020) 095001.
[36] A.K. Weaver, et al., Environmental factors influencing COVID-19 incidence and severity, Annu. Rev. Publ. Health 43 (1) (2022) 271–291.